The Effect of Crystal Packing and Re(IV) Ions on the Magnetisation Relaxation of [Mn6]-Based Molecular Magnets

ChemPubSoc Europe

DOI: 10.1002/chem.201500439

CHEMISTRY
A European Journal
Full Paper

Magnetic Properties | *Hot Paper*

The Effect of Crystal Packing and Re^{IV} Ions on the Magnetisation Relaxation of $[Mn_6]$-Based Molecular Magnets

José Martínez-Lillo,*[a] Joan Cano,[b] Wolfgang Wernsdorfer,[c] and Euan K. Brechin*[a]

Abstract: The energy barrier to magnetisation relaxation in single-molecule magnets (SMMs) proffers potential technological applications in high-density information storage and quantum computation. Leading candidates amongst complexes of 3d metals ions are the hexametallic family of complexes of formula $[Mn_6O_2(R\text{-}sao)_6(X)_2(solvent)_y]$ ($saoH_2$ = salicylaldoxime; X = mono-anion; y = 4–6; R = H, Me, Et, and Ph). The recent synthesis of cationic $[Mn_6][ClO_4]_2$ family members, in which the coordinating X ions were replaced with non-coordinating anions, opened the gateway to constructing families of novel $[Mn_6]$ salts in which the identity and nature of the charge balancing anions could be employed to alter the physical properties of the complex. Herein we demonstrate initial experiments to show that this is indeed possible. By replacing the diamagnetic ClO_4^- anions with the highly anisotropic Re^{IV} ion in the form of $[Re^{IV}Cl_6]^{2-}$, the energy barrier to magnetisation relaxation is increased by up to 30%.

Introduction

In the multidisciplinary field of molecule-based magnetism, the structural and magnetic properties of molecular magnets have been thoroughly investigated for their fundamentally interesting chemistry and physics that can potentially provide a gateway for the discovery of new physical phenomena and application in a diverse array of technological applications.[1–9] These can include quantum information processing,[10–12] cryogenic refrigeration[13,14] and molecular spintronics.[15] In molecules of the 3d transition metal ions, slow relaxation of the magnetisation in single-molecule magnets (SMMs)—as evidenced through temperature and sweep rate dependent hysteresis loops in magnetisation versus field studies—originates from a large-spin ground state (S) and a significant negative axial zero-field splitting (zfs) of that ground state (D), with the upper limit of the energy barrier (U) for the reorientation of the magnetisation vector given by $S^2|D|$ or $(S^2-1/4)|D|$ for integer and half-integer S values, respectively.

In recent years, a large body of work has involved the use of derivatised salicylaldoxime ($R\text{-}saoH_2$)[16–22] and salicylamidoxime ($H_2N\text{-}saoH_2$)[23–27] ligands in Mn^{III} coordination chemistry. This has led to the isolation of an extensive family of hexanuclear Mn^{III} SMMs, many of them possessing spin ground states as large as S = 12 and energy barriers to magnetisation reversal and blocking temperatures that are the largest reported for polynuclear transition-metal complexes.[16–23] The solution stable, magnetically tuneable $[Mn_3]$ building blocks from which these hexamers are constructed are appealing candidates for building novel molecule-based magnets, because nearest neighbour magnetic exchange (J) is controlled by the twisting of the Mn-N-O-Mn torsion angle, and this in turn is controlled through simple organic chemistry through derivitisation of the oxime ligand.[16–27]

Very recently, the first example of a cationic salicylamidoxime-based $[Mn_6]^{2+}$ SMM of formula $[Mn_6(\mu_3\text{-}O)_2(H_2N\text{-}sao)_6(py)_6(EtOH)_2][ClO_4]_2\cdot 4EtOH$ possessing a S = 12 ground state, was reported.[26,27] The preparation of this cationic $[Mn_6]^{2+}$ complex opens a plethora of new and appealing synthetic routes that can be easily exploited to obtain advanced, potentially multi-functional magnetic materials, since the identity and nature of the anion can be deliberately employed to control, for example, solubility, reactivity, stability and substrate specificity, but also because the cationic cluster produced can be charged balanced through the incorporation of anions that bring another physical property or functionality to the material, such as conductivity, luminescence or paramagnetism. In this report we employ the Re^{IV} in the form of the $[Re^{IV}Cl_6]^{2-}$ anion to generate $[Mn_6][ReCl_6]$ salts.

The magnetic properties of hexachlororhenate(IV) salts have been studied for decades.[28–36] It is well-known that significant

[a] *Dr. J. Martínez-Lillo, Prof. E. K. Brechin*
EaStCHEM School of Chemistry, The University of Edinburgh
David Brewster Road, Edinburgh, EH9 3FJ, Scotland (UK)
E-mail: ebrechin@staffmail.ed.ac.uk
lillo@uv.es

[b] *Dr. J. Cano*
Fundació General de la Universitat de València (FGUV)
Instituto de Ciencia Molecular (ICMol), Universitat de València
C/Catedrático José Beltrán n° 2, 46980 Paterna (València) (Spain)

[c] *Dr. W. Wernsdorfer*
Institut Néel-CNRS
BP 166, 25 Avenue des Martyrs, 38042 Grenoble Cedex 9 (France)

Supporting information for this article is available on the WWW under http://dx.doi.org/10.1002/chem.201500439.

magnetic interactions between the paramagnetic Re^{IV} centres ($5d^3$ ion) in hexachlororhenate(IV) salts of univalent, diamagnetic cations[28–31] are transmitted through Re–Cl···Cl–Re intermolecular contacts,[28–32] or in some instances by Re–Cl···(H_2O)···Cl–Re type pathways.[33] The use of paramagnetic counter cations has also provided new insights into the magnetic properties of this family of materials, with magnetostructural studies on hexachlororhenate(IV) salts of organic radicals,[34] ferrocenium[35] and ruthenium(III)[36] cations revealing the occurrence of fascinating magnetic phenomena, such as spin canting.[36] The use of cationic nanomagnets as countercations in hexachlororhenate(IV) salts has, however, never been explored. Herein we report the effect of introducing the Re^{IV} ion as $[ReCl_6]^{2-}$ into salicylamidoxime-based $[Mn_6]$ systems with the aim of inducing changes in the magnetisation relaxation dynamics. To that end, two compounds, of formula $[Mn^{III}_6(\mu_3\text{-}O)_2(H_2N\text{-}sao)_6(py)_6(H_2O)_2][Re^{IV}Cl_6]\cdot 4\,py\cdot 4\,CH_3CN\cdot 4\,H_2O$ (**1**) and $\{[Mn^{III}_6(\mu_3\text{-}O)_2(H_2N\text{-}sao)_6(py)_6(H_2O)_2][Mn^{III}_6(\mu_3\text{-}O)_2(H_2N\text{-}sao)_6(py)_6(EtOH)_2][Re^{IV}Cl_6]_2\}\cdot 4\,CH_3CN\cdot 12\,H_2O$ (**2**), have been magnetostructurally studied. The two salts exhibit different crystal packing, and display markedly different magnetic properties.

Results and Discussion

Description of the structures of 1 and 2

Compounds **1** and **2** are $[Mn_6][ReCl_6]$ salts that crystallise in the space groups $P2/n$ and $P\bar{1}$, respectively. Their structures consist of the hexanuclear $[Mn_6]^{2+}$ cations, mononuclear $[ReCl_6]^{2-}$ anions and CH_3CN (**1** and **2**), H_2O (**1** and **2**) and pyridine (**1**) solvent molecules of crystallisation, self-assembled through hydrogen-bonding interactions (Figure 1 and Figure S1 in the Supporting Information).

Each Re^{IV} ion in **1** and **2** is six-coordinate and bonded to six chlorides in a regular octahedral geometry. No significant differences are seen in the Re–Cl bond lengths (the average value being 2.335(1) Å and 2.360(1) Å in **1** and **2**, respectively), in agreement with those found in previously reported compounds containing the $[ReCl_6]^{2-}$ anion.[31–36] Each cationic $[Mn_6(\mu_3\text{-}O)_2(H_2N\text{-}sao)_6(py)_6(L)_2]^{2+}$ [L = H_2O (**1** and **2**) and EtOH (**2**)] complex contains two symmetry equivalent $\{Mn_3(\mu_3\text{-}O)\}$ triangular moieties, which are linked by two phenolate and two oximate oxygen atoms and are related by an inversion centre. In the asymmetric unit of **2**, two different $\{Mn_3(\mu_3\text{-}O)\}$ subunits occur that generate two crystallographically independent $[Mn_6]^{2+}$ molecules (**2a** and **2b**). Each edge of the triangle is spanned by the -N-O- moiety of the oxime ligand, with the central O^{2-} ion displaced 0.078 (**1**), 0.074 (**2a**) and 0.067 Å (**2b**) above the plane of the $\{Mn_3\}$ triangle, towards the terminally coordinated pyridine molecules. The hexametallic cores in **1** and **2** are therefore rather similar to their cationic oxime-based $[Mn_6][ClO_4]_2$ relatives.[26–27] The six Mn^{III} ions exhibit distorted octahedral geometries with their Jahn–Teller (JT) axes approximately perpendicular to the $\{Mn_3(\mu_3\text{-}O)\}$ planes (Figure 1a and Figure S1 in the Supporting Information). The remaining coordination site on the third Mn ion (and symmetry equivalent) is occupied by one H_2O (**1** and **2**) or EtOH (**2**) molecule. The Mn-N-O-Mn torsion angles of the $[Mn^{III}_3(\mu_3\text{-}O)(H_2N\text{-}sao)_3]$ triangular units are 37.2, 28.2 and 22.4° for **1** and 39.2, 34.6 and 34.3° and 39.1, 32.6 and 27.0° for **2** (**2a** and **2b**, respectively).

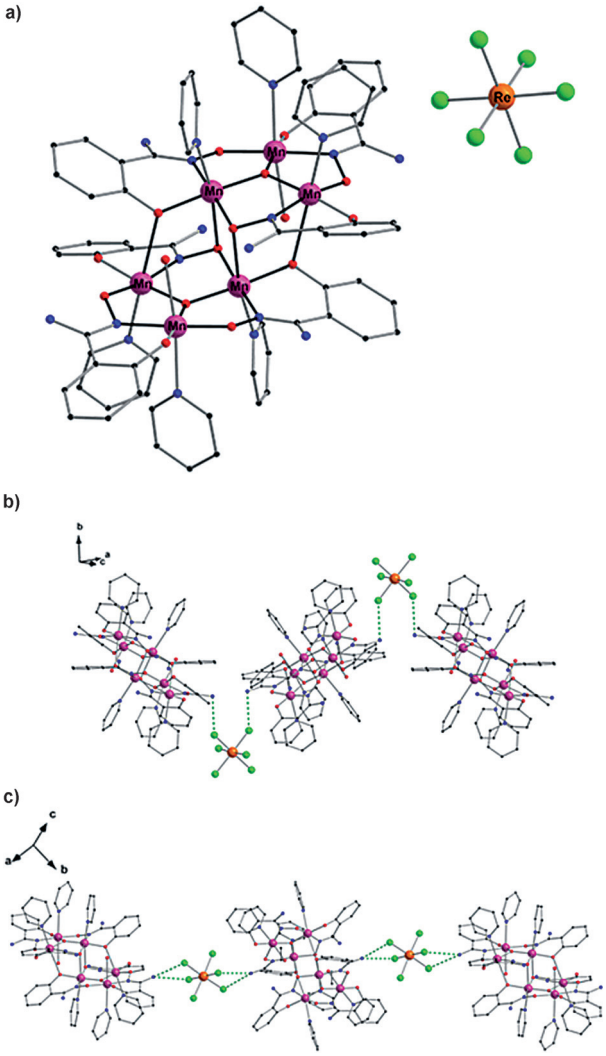

Figure 1. a) Perspective drawing of the $[Mn_6(\mu_3\text{-}O)_2(H_2N\text{-}sao)_6(py)_6(H_2O)_2]^{2+}$ cation and the $[ReCl_6]^{2-}$ anion of **1**. b) and c) View of a fragment of the crystal packing of **1** (b) and **2** (c) showing the relative arrangement of $[Mn_6]^{2+}$ cations and $[ReCl_6]^{2-}$ anions and the shortest Cl···N distances (dashed lines). H atoms and solvent molecules of crystallisation have been omitted for clarity. Colour code: orange, Re; pink, Mn; green, Cl; red, O; blue, N; black, C.

In the crystal packing of **1** and **2**, $[Re^{IV}Cl_6]^{2-}$ anions sit between neighbouring $[Mn^{III}_6]^{2+}$ cations and are hydrogen-bonded to the -NH_2 groups on the salicylamidoxime ligands of each (the shortest Cl···N distance being approximately 3.27 and 3.23 Å in **1** and **2**, respectively), linking them into chains (Figure 1b and 1c). The shortest intrachain Re^{IV}···Mn^{III} distances being 7.126(1) Å (**1**) and 7.743(1) (**2**) Å. Additionally, short Cl···H–C contacts occur between $[Re^{IV}Cl_6]^{2-}$ anions and the aromatic rings of the pyridine molecules terminally ligated to the Mn ions (range ca. 2.79–3.09 Å), which generate 2D networks (Figure 2a and Figure S2 in the Supporting Information). These sheets are separated from each other with the closest C···C interactions being of the order of 3.5 Å (Figure S2 in the Sup-

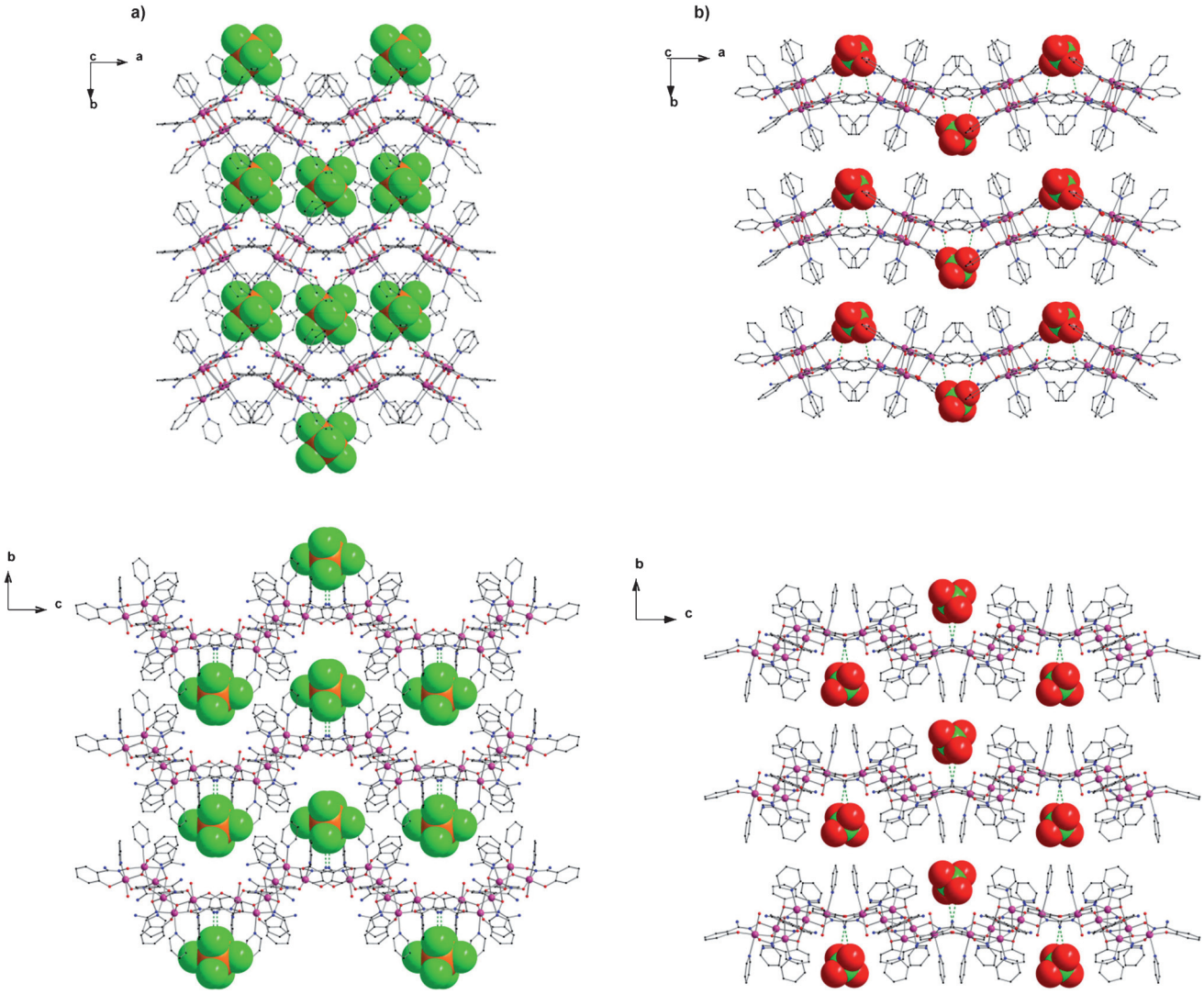

Figure 2. View of the crystal packing of a) **1** and b) **3** showing the similar arrangement of the paramagnetic $[ReCl_6]^{2-}$ and diamagnetic ClO_4^- anions as a space-filling model along the *c* (top) and *a* (bottom) axes. H atoms, solvent molecules of crystallisation, and 4-*tert*-butyl groups in **3** have been omitted for clarity. Colour code: orange, Re; pink, Mn; green, Cl; red, O; blue, N; black, C.

porting Information). Some of the remaining -NH_2 groups are also hydrogen-bonded to CH_3CN (**1** and **2**), H_2O (**1** and **2**) and pyridine (**1**) solvent molecules of crystallisation. It is important to note here that crystal packing effects are very important in this family of molecules, since intermolecular interactions are, in part, responsible for the intramolecular geometries—particularly the angles—within the $[Mn_6]$ unit. These, in turn, are responsible for the molecular magnetic behaviour and this particular family shows high sensitivity to such changes, as definitely proved through detailed solution-based susceptibility measurements.[37]

Magnetic properties and DFT of 1 and 2

Direct current (dc) susceptibility studies

The dc magnetic susceptibility measurements were carried out on microcrystalline samples of **1** and **2** in the 5–300 K temperature range in an external magnetic field of 0.1 T. The $\chi_M T$

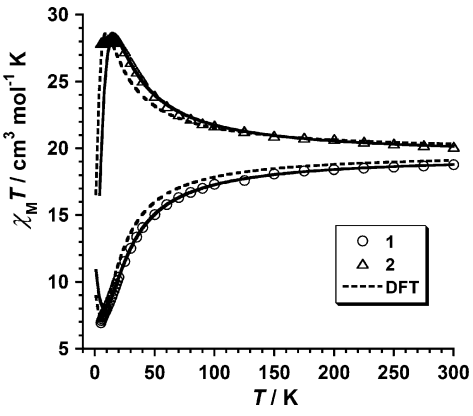

Figure 3. Thermal variation of the $\chi_M T$ product for **1** and **2**. The solid lines represent the best-fit of the experimental data for compounds **1** (o) and **2** (Δ). The dotted lines are theoretical curves generated through DFT calculations. See text for details.

versus T plots are given in Figure 3, with compounds **1** and **2** displaying markedly different thermal dependencies. Values of 18.8 and 20.1 $cm^3 mol^{-1} K$ at room temperature for **1** and **2** are, respectively, lower and higher than that expected (19.6 $cm^3 mol^{-1} K$) for six Mn^{III} ions ($S=2$, $g=2.0$) plus one Re^{IV} ion ($S=3/2$, $g=1.8$), assuming no interaction between the metal ions at this temperature (Figure 3). This is suggestive of dominant antiferromagnetic exchange in **1**, and dominant ferromagnetic exchange in **2**. This is supported by the decrease and increase of the $\chi_M T$ product when the samples are cooled down for **1** and **2**, respectively. For **1**, the $\chi_M T$ product reaches a low temperature value of 6.7 $cm^3 mol^{-1} K$. On the other hand, $\chi_M T$ for **2** reaches a maximum followed by a plateau corresponding to values of 28.4 and 27.9 $cm^3 mol^{-1} K$. However, the maximum value is too low for what would be expected for a system in which all local spins were aligned in a parallel fashion, suggesting that antiferromagnetic exchange may be also present—and this could potentially be intra and/or intermolecular in nature.

Density functional theory (DFT) calculations were employed to evaluate any possible magnetic exchange between the Re^{IV} and Mn^{III} ions in these systems. It is well-known that intermolecular magnetic interactions between $[ReCl_6]^{2-}$ anions can be non-negligible because of the strong π spin delocalization from the Re^{IV} ion onto the chlorine ions, mediating an interaction between spin densities on neighbouring molecules.[32] However, in **1** and **2**, the $[ReCl_6]^{2-}$ anions are well isolated from each other and can only interact with the closer $[Mn_6]$ moieties. As indicated above, there are Re^{IV}–Cl···$[Mn_6]$ interactions through Cl···H–N and Cl···H–C contacts that lead to the formation of chains and 2D networks, respectively (Figure 1 b,c and Figure S2 in the Supporting Information). In **2** there are more intermolecular interactions leading to a more complex network, hence we restrict discussion to complex **1**, and extend the derived conclusions to complex **2**. Calculations were performed on the cationic $[Mn^{III}_6(\mu_3\text{-}O)_2(H_2N\text{-}sao)_6(py)_6(H_2O)_2]^{2+}$ species of **1**, which is also present in compound **2** (Figure S1 in the Supporting Information).

In **1**, the first type of Re^{IV}–Cl···$[Mn_6]$ interaction, involving three short Cl···H–C contacts between the $[Re^{IV}Cl_6]^{2-}$ anion and the pyridine molecule terminally bonded to Mn(1) (Figure S3a in the Supporting Information), can be directly correlated to just one magnetic exchange between the Mn^{III} and Re^{IV} ions through this pathway, and a weak ferromagnetic exchange $J_{Re,Mn(1)} = +0.3\ cm^{-1}$ was computed. However, through the second type of Re^{IV}–Cl···$[Mn_6]$ interaction, which involves both the pyridine molecule on Mn(3) (Cl···H–C contacts) and the $-NH_2$ group from the salicylamidoxime molecule bonded to Mn(2) (Cl···H–N contact; see Figure S3b in the Supporting Information), two weak antiferromagnetic exchange interactions are revealed, $J_{Re,Mn(3)} = -0.07\ cm^{-1}$ and $J_{Re,Mn(2)} = -0.15\ cm^{-1}$. These weak exchange interactions contrast with those reported between neighbouring $[ReCl_6]^{2-}$ molecules,[31,33] as expected, since spin delocalization from the Mn^{III} ion to its peripheral ligands is much poorer than that observed for the Re^{IV} ion (Figure 4).

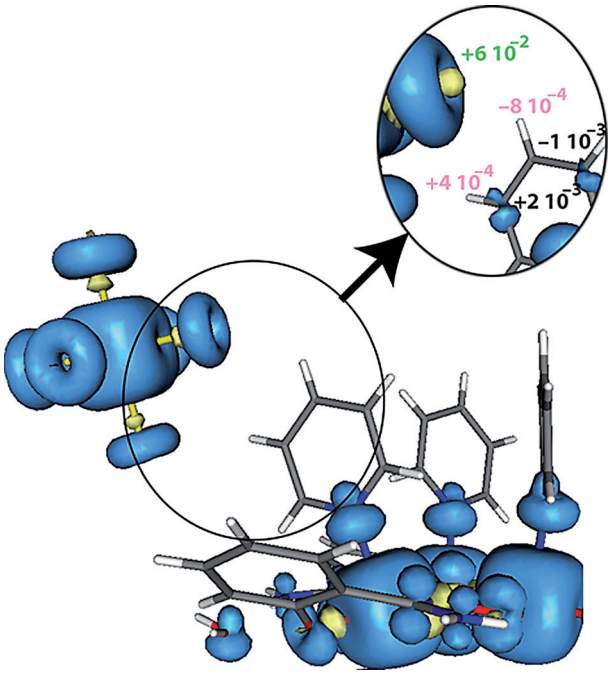

Figure 4. View of the calculated spin density for the $S=27/2$ spin configuration of the $[Mn_6]^{2+}$ and $[ReCl_6]^{2-}$ couple in **1**, highlighting the region involved in the intermolecular magnetic interaction. The isodensity surface corresponds to a cut-off value of 0.002 and 0.0004 e $bohr^{-3}$ for the inset. Blue and yellow isosurfaces correspond to positive and negative regions of spin density, respectively. The numerical values are the atomic spin densities (in e) for the involved atoms. On the H atoms of the pyridine ligand bonded to Mn, these are two orders less than those on the closer chlorine atoms. Solvent molecules and peripheral atoms have been omitted for clarity.

Since the electronic effects of the $[ReCl_6]^{2-}$ anion on the $[Mn_6]^{2+}$ complex are weak, intramolecular Mn^{III}–Mn^{III} magnetic exchange interactions were calculated on isolated $[Mn_6]^{2+}$ complexes of **1** and **2**, removing the $[ReCl_6]^{2-}$ anion. As indicated in the structure description, the $[Mn_6]^{2+}$ complexes are constructed from the stacking of two simple oxo-centred $\{Mn^{III}_3\}$ triangular building blocks, coupled together to form the well-known $[Mn^{III}_6]$ structure. The Mn^{III} ions within these triangular subunits are connected to each other by means of two exchange pathways, corresponding to the -N-O- moiety of the oxime group along each edge of the triangle and an oxo group (O^{2-}) at the centre of the triangle. The three Mn^{III} ions are inequivalent by symmetry due to the presence of one coordinated solvent molecule and one oxime or phenoxo oxygen atom in the axial position of each Mn^{III} ion. The lack of symmetry ensures three different magnetic exchange interactions per triangular subunit. Moreover, in both **1** and **2**, the $\{Mn_3\}$ moieties are connected to each other through two oximic oxygen atoms and two -N-O- oxime groups, generating two additional magnetic exchange pathways (Figure S4 in the Supporting Information).

It has been demonstrated that the broken-symmetry approach applied to calculations based on DFT can provide accurate values of magnetic coupling constants.[38–41] Thus, by employing an Heisenberg Hamiltonian of the form $\hat{H} = -J\hat{S}_i\hat{S}_j$ (see Supporting Information and Figure S4), theoretical values of

the five proposed magnetic exchange couplings can be obtained for **1** and **2** (Table S1 in the Supporting Information). In agreement with the observed experimental behaviour, these results confirm the presence of dominant antiferro- and ferromagnetic exchange in **1** and **2**, respectively. Their magnitude and nature can be understood through consideration of pertinent structural features and the arrangement of the Jahn–Teller (JT) axis of the Mn^{III} ions, as described in the Supporting Information. In summary, the ferromagnetic nature of J_5 is a result of orthogonality between spin densities delocalized on the magnetic pathways from the dz^2 orbital of the Mn^{III} ions (Figure S5 in the Supporting Information). In all other cases, the magnetic exchange interactions behave according to a previously reported magneto-structural correlation with the Mn-N-O-Mn (τ) dihedral angle (Figure S6 in the Supporting Information).[42] The spin ground state and the energy and S momenta of the first excited states evaluated from these exchange interactions for **1**, **2a** and **2b** are listed in Table S2 in the Supporting Information. In each case, a different ground state was found, but with the excited states very close in energy, permitting a change of ground state through small modifications of the magnitude of J. Although the $J_{1,3}$ values determine the spin ground state of the $\{Mn_3\}$ subunits, they can only impose a magnetic ground state on the $[Mn_6]^{2+}$ complex when ferromagnetic exchange is predominant in J_4 and J_5. Otherwise, a singlet ground state will always be found.

Given that the magnetic exchange between Mn^{III} and Re^{IV} ions is relatively weak and should have little significant influence on the $\chi_M T$ product in the explored temperature range, it could be assumed that the $[Mn_6]^{2+}$ and $[ReCl_6]^{2-}$ units are uncoupled. In that sense, theoretical simulations from the so-obtained J values were performed using fixed values of g ($g_{Mn}=2.0$ and $g_{Re}=1.9$), which are similar to those found in the literature (dotted lines in Figure 3).[23,25,42] In **1** and **2**, the agreement between theoretical and experimental simulations is excellent. For this reason, even though there are a large number of independent parameters (g, J and D), tentative fittings were performed (solid lines in Figure 3), albeit with the caveat that caution should be exercised and the numbers should be taken as a guide only. Above 15 K the influence on the $\chi_M T$ product from the magnetic anisotropy of the Mn^{III} and Re^{IV} ions should not be significant, and can be excluded. The $\chi_M T$ versus T curves can be reproduced with the following parameters: $g_{Mn}=1.99$, $g_{Re}=1.89$, $J_1=-0.3\ cm^{-1}$, $J_2=-4.4\ cm^{-1}$, $J_3=-0.8\ cm^{-1}$, $J_4=-2.8\ cm^{-1}$, $J_5=+4.5\ cm^{-1}$ and $F=5.0\times10^{-6}$ for **1** and $g_{Mn}=1.98$, $g_{Re}=1.89$, $J_1=+2.7\ cm^{-1}$, $J_2=+2.0\ cm^{-1}$, $J_3=+3.3\ cm^{-1}$, $J_4=-2.2\ cm^{-1}$, $J_5=+2.9\ cm^{-1}$ and $F=1.4\times10^{-5}$ for **2**, F being the agreement factor defined as $F=\Sigma[(\chi_M T)_{exptl}-(\chi_M T)_{calcd}]^2/\Sigma[(\chi_M T)_{exptl}]^2$. The obtained g and J values are similar to those found previously by DFT calculations on $[Mn_6]$ systems.[23,25,42] Moreover, the g-factor values for Mn^{III} and Re^{IV} obtained from the fit fall into the typical range reported for these metal ions. For **2**, in which two cationic $[Mn_6]^{2+}$ complexes coexist (**2a** and **2b**), the fit was performed considering only one cationic entity (**2a**).

Alternating current (ac) susceptibility studies

The ac susceptibility measurements were performed on samples of **1** and **2** in the 2–10 K temperature range in zero applied dc field and a 3.5 G ac field oscillating at 50–1000 Hz. **1** and **2** exhibit out-of-phase ac signals in their χ''_{ac} vs. T plots (Figure 5), which are consistent with SMM behaviour. Indeed, a clear frequency-dependent decrease of the χ''_{ac} maxima is observed. These data were fitted to the Arrhenius equation [$\tau=\tau_o\exp(U_{eff}/k_BT)$, in which τ_o is the pre-exponential factor, τ is the relaxation time, U_{eff} is the energy barrier to the relaxation of

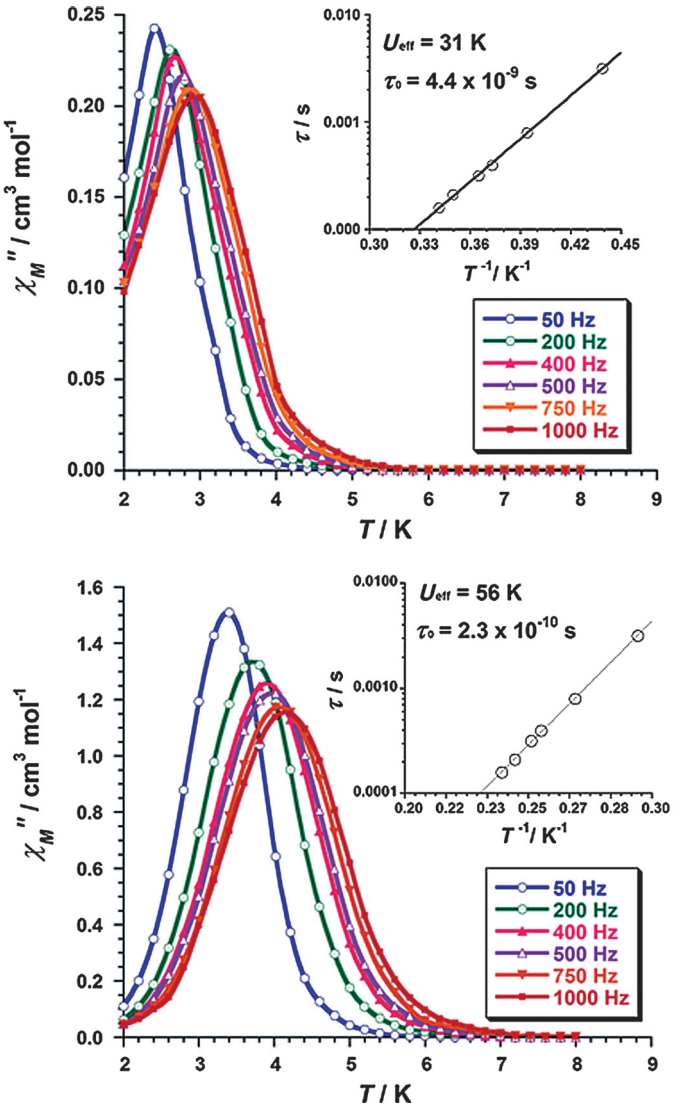

Figure 5. Out-of-phase ac susceptibility (χ''_{ac}) versus T plot for compounds **1** (top) and **2** (bottom). The insets show the Arrhenius best-fit plot. The ac susceptibility measurements were performed in zero applied dc field and a 3.5 G ac oscillating field with temperature and frequency ranges of 2–8 K and 50–1000 Hz, respectively.

the magnetisation and k_B is the Boltzmann constant] and plotted in the insets of Figure 5. The obtained values for τ_o and U_{eff} are 4.4×10^{-9} s and 31 K for **1** and 2.3×10^{-10} s and 56 K for **2**, which fall into the range for previously reported salicylamidoxime-based [Mn_6] complexes.[23–27] The U_{eff} value for **1** is higher than that of the structurally analogous compound $[Mn_6][ClO_4]_2$ ($U_{eff}=25$ K), of formula $[Mn_6(\mu_3\text{-}O)_2(H_2N\text{-}sao)_6(tpy)_6(H_2O)_2](ClO_4)_2\cdot2\,tpy\cdot4\,H_2O\cdot2\,EtOH$ (**3**) (tpy = 4-tert-butylpyridine), which crystallises in the same space group as **1**, packs in a similar fashion (see Figure 2 and Figure S7 in the Supporting Information) and possesses a broadly similar range of Mn-N-O-Mn torsion angles (37.2, 28.2 and 22.4° in **2** vs. 37.9, 31.8 and 17.9° in **3**).[27] The same trend is observed when we compare the U_{eff} value of **2** with that of the structurally analogous $[Mn_6(\mu_3\text{-}O)_2(H_2N\text{-}sao)_6(py)_6(EtOH)_2][ClO_4]_2\cdot4\,EtOH$ (**4**) with $U_{eff}=40$ K, which also packs in a similar fashion (see Figure S8 in the Supporting Information) and possesses a similar range of Mn-N-O-Mn torsion angles (39.2, 34.6 and 34.3° and 39.1, 32.6 and 27.0° in **2** vs. 42.0, 39.4 and 30.8° in **4**). These results indicate that the energy barrier to magnetisation reversal in the cationic $[Mn_6]^{2+}$ complexes has been increased (by approximately 20% in **1** and 30% in **2**) simply through replacing the diamagnetic ClO_4^- anion with the paramagnetic and anisotropic $[Re^{IV}Cl_6]^{2-}$ anion.

The factors that govern this change in the relaxation dynamics of these systems are, however, extremely difficult to extract, since it is a many-body problem. One possible cause is simply the occurrence of 2D or 3D magnetic networks built from the intermolecular magnetic interactions, although the $J_{Re,Mn}$ magnetic exchange interactions are too weak to promote magnetic order in the temperature range studied, as shown in the experimental magnetic susceptibility. Structural changes in the [Mn_6] cluster unit could also explain the increase in the U_{eff}, but the experimentally observed structural changes appear to be too small to have such a dramatic effect. From a theoretical point of view, it is possible to qualitatively study the origins of this behaviour. In a previous DFT study on [Mn_6] complexes it was shown that the energy barrier is similar in all *S* spin states of a certain system.[43] This fact is also supported by the Wigner–Eckardt theorem for systems with paramagnetic centres showing parallel *z*-axis orientations for the anisotropy tensor, which is indeed the case of [Mn_6], in which the Jahn–Teller (JT) axes of the Mn^{III} ions are quasi-parallel.[44] Thus, the estimation of the energy barrier to magnetisation relaxation from the *D* parameter can be performed on the ferromagnetic state ($S=12$ for Mn_6). For the $[Mn_6]^{2+}$ complex in **1**, the two different $[Mn_6]^{2+}$ entities in **2**, and the complex from the perchlorate salt of **4**, this leads to quasi-identical energy barriers in all cases—the U_{eff} value being 46.7, 46.4, 46.3 and 46.9 K, respectively (Table S4 in the Supporting Information). Although other energy barriers were found using different approaches to include the spin-orbit coupling, the four studied $[Mn_6]^{2+}$ unities always showed similar values (Table S4 in the Supporting Information). Although structural changes in $[Mn_6]^{2+}$ as a cause of the large modification in the relaxation dynamics certainly cannot be ruled out, it seems likely that the role of the $[Re^{IV}Cl_6]^{2-}$ anion is non-innocent. Indeed, the calculation of the *D* and *E*/*D* parameters on **1**, including the $[Re^{IV}Cl_6]^{2-}$ anion, afford $U_{eff}=63.8$ K, an increase of ca. 27% from that calculated only for the $[Mn_6]^{2+}$ entity (Table S4 in the Supporting Information). This increase of the theoretically obtained U_{eff} value is very close to that experimentally found (ca. 20 (**1**) and ca. 30% (**2**)).

In order to probe this possibility further, micro-SQUID measurements were performed on single crystals of **1** and **2** with the field applied along the easy axis of magnetization in both cases.[45] Hysteresis loops at varying temperatures and sweep rates are shown in Figure 6, and Figures S9 and S10 in the Supporting Information, and suggest rather complex behaviour. Compound **1** exhibits a fast relaxing tunnel transition at $H=0$, which is not observed for **2**, suggesting that the packing of the molecules in the crystal of **1** exerts less influence on the low temperature magnetic behaviour of the individual [Mn_6] molecules than that in **2**, consistent with the extended structure in the crystals of both. Indeed, significant intermolecular interactions would be expected to produce an exchange-bias

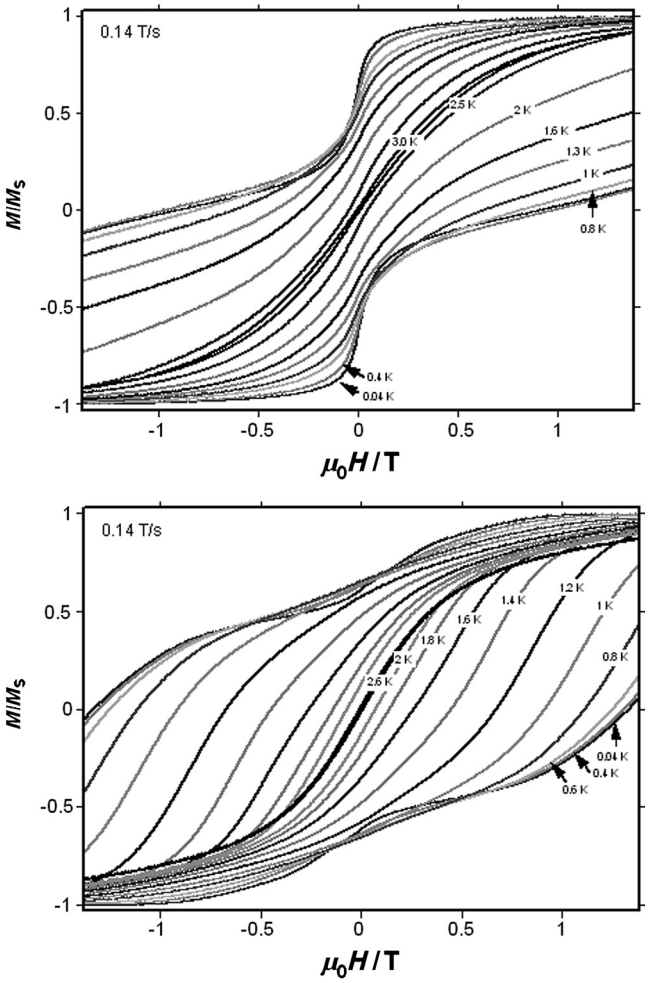

Figure 6. Magnetisation (*M*) (plotted as a fraction of the M_S maximum value) versus applied field (μ_0H) recorded on a single crystal of **1** (top) and **2** (bottom). The resulting loops are shown at different temperatures (0.04–3.00 K).

effect which would shift the resonance away from zero-field—as is clearly seen for **2**. Such intermolecular effects include both the influence of the solid state packing on the intramolecular geometry of the $[Mn_6]^{2+}$ cations (the changes in Mn-N-O-Mn torsion angles are particulalry important for this class of compound), and the intermolecular interactions between the $[Mn_6]$ molecules mediated by the Re^{IV} ions. Likely both effects have some influence, and one could speculate that the dominant effect in **1** relates to intramolecular geometries with the influence of the Re ion more pertinent in **2**, but deconvoluting which is dominant and more important is rather difficult.

Conclusion

Reaction of $Mn[NO_3]_2{\cdot}4H_2O$ with H_2N-saoH_2 and pyridine in the presence of $[ReCl_6]^{2-}$ and NEt_3 in CH_3CN results in the formation of dark green crystals of $[Mn^{III}_6(\mu_3\text{-}O)_2(H_2N\text{-}sao)_6(py)_6(H_2O)_2][Re^{IV}Cl_6]{\cdot}4\,py{\cdot}4\,CH_3CN{\cdot}4\,H_2O$ (**1**) and $\{[Mn^{III}_6(\mu_3\text{-}O)_2(H_2N\text{-}sao)_6(py)_6(H_2O)_2][Mn^{III}_6(\mu_3\text{-}O)_2(H_2N\text{-}sao)_6(py)_6(EtOH)_2][Re^{IV}Cl_6]_2\}{\cdot}4\,CH_3CN{\cdot}12\,H_2O$ (**2**). These synthetic procedures are non-trivial, since they are performed in basic medium and in the presence of O^{2-} ions, despite the fact that under such conditions the Re^{IV} ion readily undergoes either oxidation or hydrolysis to form Re^{V} or Re^{VII} species, respectively.[46] The synthesis of cationic $[Mn_6]^{2+}$ complexes is an important milestone for this family of SMMs, because it makes possible the construction of multifunctional salts in which the identity and nature of the anion can be exploited to enhance or completely change the physical properties of the complex. Here we have demonstrated our initial experiments in this regard by replacing the diamagnetic ClO_4^- anions with the highly anisotropic Re^{IV} ion in the form of $[Re^{IV}Cl_6]^{2-}$, generating $[Mn_6][ReCl_6]$ salts. Our results suggest that the $[Re^{IV}Cl_6]^{2-}$ anion can 1) induce structural distortions of the Mn-N-O-Mn bridges through hydrogen-bonding interactions, 2) mediate magnetic exchange pathways with the $[Mn_6]^{2+}$ cations and 3) provide increased anisotropy to the system. The complexity of our systems makes it hard to deconvolute the relative importance of the various structural and electronic parameters in the resulting magnetic behaviour, but what is clear is that the magnetic behaviour has been modified. The relevance of hydrogen-bonding interactions generating weak ferromagnetic exchange between $[Re^{IV}Cl_6]^{2-}$ complexes has previously been reported,[33] but this is the first time that it has been observed between the Re^{IV} ion and a different paramagnetic metal ion (Mn^{III}). Clearly there remains a myriad of other anions, for example 4d or 5d metal complexes, polyoxometalates, spin crossover materials, and other SMMs, that await examination.

Experimental Section

Synthesis of 1 and 2: All manipulations were performed under aerobic conditions, using chemicals as received from Sigma-Aldrich. Type 3 Å molecular sieves were used to dry the CH_3CN before use. The $[NBu_4]_2[ReCl_6]$ precursor was prepared following the literature procedure.[32] $Mn[NO_3]_2{\cdot}4H_2O$ (0.20 g, 0.8 mmol) was dissolved with continuous stirring in CH_3CN (20 mL). H_2N-saoH_2 (0.12 g, 0.8 mmol) was then added, followed by pyridine (5 mL, 62.0 mmol) and NEt_3 (0.05 mL, 3.58 mmol). $[NBu_4]_2[ReCl_6]$ (0.67 g, 0.8 mmol) dissolved in CH_3CN (5 mL) was added dropwise, and the dark green solution was left to evaporate in a fumehood at room temperature. Dark green crystals of **1**, suitable for X-ray diffraction studies, were formed in 1 day. Compound **2** was prepared as **1** but by adding less pyridine (1 mL, 12.4 mmol) in a 4:1 CH_3CN/EtOH (25 mL, v/v) mixture.

Data for 1: Yield: 35%; elemental analysis calcd (%) for $C_{72}H_{70}O_{16}N_{18}Cl_6Mn_6Re$ (**1**): C 39.8, H 3.3, N 11.6; found: C 40.1, H 3.4, N 11.9; IR (ATR): $\tilde{\nu}=3548$ (w), 3504 (w), 3427 (m), 3300 (w), 3064 (w), 1597 (vs), 1574 (s), 1527 (s), 1483 (m), 1441 (vs), 1314 (s), 1252 (s), 1148 (m), 1069 (m), 1022 (s), 1005 (s), 879 (s), 832 (w), 757 (s), 701 (s), 677 (m), 643 cm^{-1} (m).

Data for 2: Yield: 55%; elemental analysis calcd (%) for $C_{148}H_{148}O_{32}N_{36}Cl_{12}Mn_{12}Re_2$ (**2**): C 40.4, H 3.4, N 11.5; found: C 40.2, H 3.7, N 11.8; IR (ATR): $\tilde{\nu}=3550$ (w), 3499 (w), 3430 (m), 3299 (w), 3063 (w), 1597 (vs), 1573 (s), 1525 (s), 1482 (m), 1440 (vs), 1314 (s), 1250 (s), 1148 (m), 1066 (m), 1021 (s), 1008 (s), 875 (s), 830 (w), 755 (s), 699 (s), 675 (m), 642 cm^{-1} (m).

X-ray data collection and structure refinement: X-ray diffraction data on single crystals of **1** and **2** were collected on a Bruker-Nonius X8 APEXII CCD area detector diffractometer with graphite-monochromated Mo-K_α radiation ($\lambda=0.71073$ Å). The structures of **1** and **2** were solved by direct methods and subsequently completed by Fourier recycling using SHELXTL. The final full-matrix least-squares refinements on F^2, minimising the function $\Sigma w(|F_o|-|F_c|)^2$.

CCDC-1029762 (**1**) and CCDC-1029763 (**2**) contain the supplementary crystallographic data for this paper. These data can be obtained free of charge from The Cambridge Crystallographic Data Centre via www.ccdc.cam.ac.uk/data_request/cif.

Magnetic studies: The dc and ac magnetic susceptibility measurements on polycrystalline samples of **1** and **2** were carried out on a Quantum Design SQUID magnetometer. The dc studies were performed in the temperature range of 5–300 K in an applied magnetic field of 0.1 T. The ac susceptibility measurements were performed in zero applied dc field and a 3.5 G ac oscillating field with temperature and frequency ranges of 2–8 K and 50–1000 Hz, respectively. Micro-SQUID measurements were performed on single crystal samples of **1** and **2** with the field applied in the direction of the easy-axis of the molecules.[45]

Computational methods: Calculations were performed through the Gaussian09 package using the B3LYP functional and the quadratic convergence approach.[48–51] Triple-ζ and double-ζ all electron basis sets, as proposed by Ahlrichs et al., were used for the metal ions and for the rest of atoms, respectively.[52,53] An approach based on the use of broken-symmetry (BS) functions built from localized orbitals was used to evaluate the energies of several spin states. The BS functions, which provide positive or negative spin densities on the paramagnetic centres, were obtained from the guess functions generated with the fragment tool implemented in Gaussian09. The full experimental geometries were used for all complexes. To stabilize the electronic surplus on the charged ligands coordinated to Mn^{III} ions, a polarizable continuum model (PCM) was introduced in the calculations. Parameters corresponding to the acetonitrile solvent were included to simulate the electronic effects of the surrounding molecules.[54] Although the B3LYP functional is widely used and checked to evaluate magnetic coupling constants in transition metal complexes, it is known that it overestimates intermolecular interactions. For this reason, the CAM-B3LYP functional (a long range corrected version of B3LYP) was used in this study.[55] To verify the results obtained for the in-

tramolecular magnetic exchange coupling between Mn^{III} ions, they were also calculated with the B3LYP functional. Similar results were obtained in both cases, although better agreement between the simulated and experimental $\chi_M T$ versus T curves were found with the CAM-B3LYP functional. In cases where the $[Re^{IV}Cl_6]^{2-}$ anion was present, double-ζ and Los Alamos effective core potentials proposed by Hay and Wadt were used for rhenium and chlorine atoms.[56–58] Also, the two-electron integrals and their derivatives were computed in such cases from a Douglas–Kroll–Hess (DKH) second-order scalar relativistic calculation.[59,60] Calculations of the zfs parameters were performed with version 3.0 of the ORCA program system.[61] A TZVP basis set proposed by Ahlrichs and tight SCF criteria were used in all cases.[53] For density functional calculations, resolution of the identity (RI) approximation with the auxiliary TZV/J Coulomb fitting basis sets and PBE functional were employed.[62] The PBE functional was used for DFT calculations.[63–64] Experimental geometries were used in the theoretical study. All calculations were done in solution, including electronic effects of the solvent (acetonitrile) by "conductor-like screening model" (COSMO).[65] DFT calculations of the zfs were carried out using the quasi-restricted orbitals.[66] The spin–orbit and spin–spin coupling operators were based on the SOMF scheme.[66] Coupled perturbed (CP)[67] and Pederson–Khanna (PK)[68] methods were used in the calculation of the zero-field splitting. Because rhenium is a heavy element, relativistic effects can be important. Thus, such effects on the electronic energy were introduced from zero-order regular approximation (ZORA).[69]

Acknowledgements

Financial support from the European Union (Marie Curie Project No. 272659), the Spanish Ministerio de Ciencia e Innovación (project CTQ2010-15364) and the Generalitat Valenciana (projects PROMETEO/2009/108, GV/2012/051 and ISIC/2012/002) is gratefully acknowledged. E.K.B. thanks the EPSRC. The authors thank Dr. G. Nichol for single-crystal X-ray diffraction measurements and Dr. D. Armentano for very useful discussions. J.M.-L. is indebted to the European Union for a postdoctoral Marie Curie Intra-European Fellowship.

Keywords: density functional calculations · magnetisation relaxation · manganese · oximes · rhenium

[1] R. Sessoli, D. Gatteschi, A. Caneschi, M. A. Novak, *Nature* **1993**, *365*, 141 – 143.
[2] W. Wernsdorfer, R. Sessoli, *Science* **1999**, *284*, 133 – 135.
[3] M. N. Leuenberger, D. Loss, *Nature* **2001**, *410*, 789 – 793.
[4] W. Wernsdorfer, N. Aliaga-Acalde, D. N. Hendrickson, G. Christou, *Nature* **2002**, *416*, 406 – 409.
[5] R. Sessoli, G. Gatteschi, *Angew. Chem. Int. Ed.* **2003**, *42*, 268 – 297; *Angew. Chem.* **2003**, *115*, 278 – 309.
[6] G. Aromí, E. K. Brechin, *Struct. Bonding (Berlin)* **2006**, *122*, 1 – 69.
[7] E. J. L. McInnes, *Struct. Bonding (Berlin)* **2006**, *122*, 69 – 102.
[8] R. Bagai, G. Christou, *Chem. Soc. Rev.* **2009**, *38*, 1011 – 1026.
[9] M. Andruh, *Chem. Commun.* **2011**, *47*, 3025 – 3042.
[10] R. E. P. Winpenny, *Angew. Chem. Int. Ed.* **2008**, *47*, 7992 – 7994; *Angew. Chem.* **2008**, *120*, 8112 – 8114.
[11] G. A. Timco, E. J. L. McInnes, R. E. P. Winpenny, *Chem. Soc. Rev.* **2013**, *42*, 1796 – 1806.
[12] G. A. Timco, T. B. Faust, F. Tuna, R. E. P. Winpenny, *Chem. Soc. Rev.* **2011**, *40*, 3067 – 3075.
[13] M. Evangelisti, F. Luis, L. J. de Jongh, M. Affronte, *J. Mater. Chem.* **2006**, *16*, 2534 – 2549.
[14] M. Evangelisti, E. K. Brechin, *Dalton Trans.* **2010**, *39*, 4672 – 4676.
[15] L. Bogani, W. Wernsdorfer, *Nat. Mater.* **2008**, *7*, 179 – 186.
[16] C. J. Milios, C. P. Raptopoulou, A. Terzis, F. Lloret, R. Vicente, S. P. Perlepes, A. Escuer, *Angew. Chem. Int. Ed.* **2004**, *43*, 210 – 212; *Angew. Chem.* **2004**, *116*, 212 – 214.
[17] C. J. Milios, A. Vinslava, P. A. Wood, S. Parsons, W. Wernsdorfer, G. Christou, S. P. Perlepes, E. K. Brechin, *J. Am. Chem. Soc.* **2007**, *129*, 8 – 9.
[18] C. J. Milios, A. Vinslava, W. Wernsdorfer, A. Prescimone, P. A. Wood, S. Parsons, S. P. Perlepes, G. Christou, E. K. Brechin, *J. Am. Chem. Soc.* **2007**, *129*, 6547 – 6561.
[19] C. J. Milios, R. Inglis, A. Vinslava, R. Bagai, W. Wernsdorfer, S. Parsons, S. P. Perlepes, G. Christou, E. K. Brechin, *J. Am. Chem. Soc.* **2007**, *129*, 12505 – 12511.
[20] C. J. Milios, R. Inglis, R. Bagai, W. Wernsdorfer, A. Collins, S. Moggach, S. Parsons, S. P. Perlepes, G. Christou, E. K. Brechin, *Chem. Commun.* **2007**, 3476 – 3478.
[21] C. J. Milios, S. Piligkos, E. K. Brechin, *Dalton Trans.* **2008**, 1809 – 1817.
[22] R. Inglis, C. J. Milios, L. F. Jones, S. Piligkos, E. K. Brechin, *Chem. Commun.* **2012**, *48*, 181 – 190.
[23] A.-R. Tomsa, J. Martínez-Lillo, Y. Li, L.-M. Chamoreau, K. Boubekeur, F. Farias, M. A. Novak, E. Cremades, E. Ruiz, A. Proust, M. Verdaguer, P. Gouzerh, *Chem. Commun.* **2010**, *46*, 5106 – 5108.
[24] J. Martínez-Lillo, L.-M. Chamoreau, A. Proust, M. Verdaguer, P. Gouzerh, *C. R. Chim.* **2012**, *15*, 889 – 894.
[25] J. Martínez-Lillo, A.-R. Tomsa, Y. Li, L.-M. Chamoreau, E. Cremades, E. Ruiz, A.-L. Barra, A. Proust, M. Verdaguer, P. Gouzerh, *Dalton Trans.* **2012**, *41*, 13668 – 13681.
[26] J. Martínez-Lillo, N. Dolan, E. K. Brechin, *Dalton Trans.* **2013**, *42*, 12824 – 12827.
[27] J. Martínez-Lillo, N. Dolan, E. K. Brechin, *Dalton Trans.* **2014**, *43*, 4408 – 4414.
[28] C. M. Nelson, G. E. Boyd, W. T. J. Smith, *J. Am. Chem. Soc.* **1954**, *76*, 348 – 352.
[29] B. N. Figgis, J. Lewis, F. E. Mabbs, *J. Chem. Soc.* **1961**, 3138 – 3145.
[30] R. Busey, E. Sonder, *J. Chem. Phys.* **1962**, *36*, 93 – 97.
[31] J. Martínez-Lillo, D. Armentano, G. De Munno, F. Lloret, M. Julve, J. Faus, *Cryst. Growth Des.* **2006**, *6*, 2204 – 2206.
[32] R. Chiozzone, R. González, C. Kremer, G. De Munno, J. Cano, F. Lloret, M. Julve, J. Faus, *Inorg. Chem.* **1999**, *38*, 4745 – 4752.
[33] J. Martínez-Lillo, D. Armentano, G. De Munno, N. Marino, F. Lloret, M. Julve, J. Faus, *CrystEngComm* **2008**, *10*, 1284 – 1287.
[34] R. González, F. Romero, D. Luneau, D. Armentano, G. De Munno, C. Kremer, F. Lloret, M. Julve, J. Faus, *Inorg. Chim. Acta* **2005**, *358*, 3995 – 4002.
[35] R. González, R. Chiozzone, C. Kremer, F. Guerra, G. De Munno, F. Lloret, M. Julve, J. Faus, *Inorg. Chem.* **2004**, *43*, 3013 – 3019.
[36] D. Armentano, J. Martínez-Lillo, *Inorg. Chim. Acta* **2012**, *380*, 118 – 124.
[37] R. Inglis, J. Bendix, T. Brock-Nannestad, H. Weihe, E. K. Brechin, S. Piligkos, *Chem. Sci.* **2010**, *1*, 631 – 636.
[38] E. Ruiz, J. Cano, S. Alvarez, P. Alemany, *J. Am. Chem. Soc.* **1998**, *120*, 11122 – 11129.
[39] E. Ruiz, J. Cano, S. Alvarez, P. Alemany, *J. Comput. Chem.* **1999**, *20*, 1391 – 1400.
[40] E. Ruiz, M. Llunell, J. Cano, P. Rabu, M. Drillon, C. Massobrio, *J. Phys. Chem. B* **2006**, *110*, 115 – 118.
[41] E. Ruiz, A. Rodríguez-Fortea, J. Cano, S. Alvarez, P. Alemany, *J. Comput. Chem.* **2003**, *24*, 982 – 989.
[42] E. Cremades, J. Cano, E. Ruiz, G. Rajaraman, C. J. Milios, E. K. Brechin, *Inorg. Chem.* **2009**, *48*, 8012 – 8019.
[43] E. Ruiz, J. Cirera, J. Cano, S. Alvarez, C. Loosec, J. Kortus, *Chem. Commun.* **2008**, 52 – 54.
[44] R. P. Scaringe, D. J. Hodgson, W. E. Hatfield, *Mol. Phys.* **1978**, *35*, 701 – 713.
[45] W. Wernsdorfer, *Adv. Chem. Phys.* **2001**, *118*, 99 – 190.
[46] G. Rouschias, *Chem. Rev.* **1974**, *74*, 531 – 566.
[47] I. Bhowmick, E. A. Hillard, P. Dechambenoit, C. Coulon, T. D. Harrisc, R. Clérac, *Chem. Commun.* **2012**, *48*, 9717 – 9719.
[48] A. D. Becke, *Phys. Rev. A* **1988**, *38*, 3098 – 3100.
[49] A. D. Becke, *J. Chem. Phys.* **1993**, *98*, 5648 – 5652.
[50] C. Lee, W. Yang, R. G. Parr, *Phys. Rev. B* **1988**, *37*, 785 – 789.

[51] Gaussian 09, Revision C.01, M. J. Frisch, G. W. Trucks, H. B. Schlegel, G. E. Scuseria, M. A. Robb, J. R. Cheeseman, G. Scalmani, V. Barone, B. Mennucci, G. A. Petersson, H. Nakatsuji, M. Caricato, X. Li, H. P. Hratchian, A. F. Izmaylov, J. Bloino, G. Zheng, J. L. Sonnenberg, M. Hada, M. Ehara, K. Toyota, R. Fukuda, J. Hasegawa, M. Ishida, T. Nakajima, Y. Honda, O. Kitao, H. Nakai, T. Vreven, J. A. Montgomery, Jr., J. E. Peralta, F. Ogliaro, M. Bearpark, J. J. Heyd, E. Brothers, K. N. Kudin, V. N. Staroverov, R. Kobayashi, J. Normand, K. Raghavachari, A. Rendell, J. C. Burant, S. S. Iyengar, J. Tomasi, M. Cossi, N. Rega, J. M. Millam, M. Klene, J. E. Knox, J. B. Cross, V. Bakken, C. Adamo, J. Jaramillo, R. Gomperts, R. E. Stratmann, O. Yazyev, A. J. Austin, R. Cammi, C. Pomelli, J. W. Ochterski, R. L. Martin, K. Morokuma, V. G. Zakrzewski, G. A. Voth, P. Salvador, J. J. Dannenberg, S. Dapprich, A. D. Daniels, Ö. Farkas, J. B. Foresman, J. V. Ortiz, J. Cioslowski, D. J. Fox, Gaussian, Inc. Wallingford CT, **2009**.
[52] A. Schäfer, H. Horn, R. Ahlrichs, *J. Chem. Phys.* **1992**, *97*, 2571 – 2577.
[53] A. Schäfer, C. Huber, R. Ahlrichs, *J. Chem. Phys.* **1994**, *100*, 5829 – 5835.
[54] J. Tomasi, B. Mennucci, E. Cancès, *J. Mol. Struct.* **1999**, *464*, 211 – 226.
[55] T. Yanai, D. P. Tew, N. C. Handy, *Chem. Phys. Lett.* **2004**, *393*, 51 – 57.
[56] P. J. Hay, W. R. Wadt, *J. Chem. Phys.* **1985**, *82*, 270 – 283.
[57] W. R. Wadt, P. J. Hay, *J. Chem. Phys.* **1985**, *82*, 284 – 298.
[58] P. J. Hay, W. R. Wadt, *J. Chem. Phys.* **1985**, *82*, 299 – 310.
[59] M. Douglas, N. M. Kroll, *Ann. Phys.* **1974**, *82*, 89 – 155.
[60] B. A. Hess, *Phys. Rev. A* **1985**, *32*, 756 – 763.
[61] F. Neese, *WIREs Comput. Mol. Sci.* **2012**, *2*, 73 – 78.
[62] R. A. Kendall, H. A. Früchtl, *Theor. Chem. Acc.* **1997**, *97*, 158 – 163.
[63] J. P. Perdew, K. Burke, M. Ernzerhof, *Phys. Rev. Lett.* **1996**, *77*, 3865 – 3868.
[64] J. P. Perdew, K. Burke, M. Ernzerhof, *Phys. Rev. Lett.* **1997**, *78*, 1396.
[65] A. Klamt, G. Schüürmann, *J. Chem. Soc. Perkin Trans. 2* **1993**, 799 – 805.
[66] F. Neese, *J. Am. Chem. Soc.* **2006**, *128*, 10213 – 10222.
[67] F. Neese, *J. Chem. Phys.* **2007**, *127*, 164112.
[68] M. R. Pederson, S. N. Khanna, *Phys. Rev. B* **1999**, *60*, 9566 – 9572.
[69] C. Chang, M. Pelissier, P. Durand, *Phys. Scr.* **1986**, *34*, 394 – 404.

Received: February 3, 2015
Published online on May 7, 2015

